RESEARCH ARTICLE
PLANETARY SCIENCE

Earth and Planetary Physics
2: 371–383, 2018
doi: 10.26464/epp2018035

Importance of electron distribution profiles to chorus wave driven evolution of Jovian radiation belt electrons

Jing Huang[1], XuDong Gu[1,2*], BinBin Ni[1,2*], Qiong Luo[1], Song Fu[1], Zheng Xiang[1], and WenXun Zhang[1]

[1]Department of Space Physics, School of Electronic Information, Wuhan University, Wuhan 430072, China;

[2]Lunar and Planetary Science Laboratory, Macau University of Science and Technology-Partner Laboratory of Key Laboratory of Lunar and Deep Space Exploration, Chinese Academy of Sciences, Macau, China

Abstract: Wave-particle interactions triggered by whistler-mode chorus waves are an important contributor to the Jovian radiation belt electron dynamics. While the sensitivity of chorus-driven electron scattering to the ambient magnetospheric and wave parameters has been investigated, there is rather limited understanding regarding the extent to which the dynamic evolution of Jovian radiation belt electrons, under the impact of chorus wave scattering, depends on the electron distribution profiles. We adopt a group of reasonable initial conditions based upon the available observations and models for quantitative analyses. We find that inclusion of pitch angle variation in initial conditions can result in increased electron losses at lower pitch angles and substantially modify the pitch angle evolution profiles of > ~500 keV electrons, while variations of electron energy spectrum tend to modify the evolution primarily of 1 MeV and 5 MeV electrons. Our results explicitly demonstrate the importance to the radiation belt electron dynamics in the Jovian magnetosphere of the initial shape of the electron phase space density, and indicate the extent to which variations in electron energy spectrum and pitch angle distribution can contribute to the evolution of Jovian radiation belt electrons caused by chorus wave scattering.

Keywords: Jovian radiation belt; whistler-mode chorus; wave-particle interactions ; electron distribution profile

Citation: Huang J., Gu X. D., Ni B. B., Luo Q., Fu S., Xiang Z., and Zhang W. X. (2018). Importance of electron distribution profiles to chorus wave driven evolution of Jovian radiation belt electrons. *Earth Planet. Phys.*, *2*(5), 371–383. http://doi.org/10.26464/epp2018035

1. Introduction

Surrounded by several moons, Jupiter is the largest planet in the solar system, with the fastest rotational speed and the strongest magnetic field. The approximate magnetic dipole of Jupiter has a small crossing angle with Jupiter's spin axis. The Jovian magnetosphere undergoes impacts from not only the solar wind but also neighboring satellites. It is well known that the radiation belts of Jupiter are the most intense of all the planets in the solar system, with the presence of highly relativistic electron populations up to 10's MeV (Bolton et al., 2002) and of > 1 MeV protons, as well as oxygen, sulfur, and sodium ions (Carr and Gulkis, 1969).

While the dynamics of energetic particle population in the Jovian magnetosphere are distinguished from terrestrial radiation belt dynamics by resulting mainly from internal factors, wave-particle interactions have long been regarded as an important factor affecting the magnetospheric energetic populations of both Earth and Jupiter. In particular, Horne et al. (2008) reported that the local acceleration by chorus waves at Jupiter may serve as a process of providing the seed electron population for further acceleration to ultra-relativistic energies in the region around $10R_J$. They also found that chorus waves can be generated and grow from the anisotropic distribution of electrons of just a few keV, and can drive the acceleration of relativistic electrons in the Jovian radiation belts in a manner similar to the Earth's radiation belts. A later study, Shprits et al. (2012), confirmed that interactions with whistler waves cause significant local acceleration of electrons at Jupiter, and indicated that the wave latitudinal distribution has a determining role in the dynamics of energetic electrons. Menietti et al. (2016) obtained a quantized distribution of chorus magnetic field intensity for use in stochastic modeling efforts, suggesting that chorus induced wave-particle interactions at Jupiter may play an even greater role than earlier proposed. De Soria-Santacruz et al. (2017) further clarified that the shape of the electron phase space density and the latitudinal extent of the chorus waves are important for both the acceleration and loss of Jovian radiation belt electrons. A very recent parametric investigation of Ni BB et al. (2018) demonstrated the importance to understanding the dynamic electron evolution in the Jovian radiation belts of reliable information regarding both the ambient magnetospheric state and wave distribution properties.

In contrast, there is rather limited understanding regarding the extent to which the dynamic evolution of Jovian radiation belt electrons, under the impact of chorus wave scattering, depends on the electron distribution profiles. Therefore, this study is direc-

Correspondence to: X. D. Gu, guxudong@whu.edu.cn
B. B. Ni, bbni@whu.edu.cn
Received 10 JUL 2018; Accepted 27 SEP 2018.
Accepted article online 28 SEP 2018.

ted towards a detailed analysis to figure out how variations of electron distribution profile contribute to the acceleration and loss processes of Jovian radiation belt electrons.

The paper is organized as follows. Section 2 describes the basic models and input parameters adopted in the context of Jupiter's magnetosphere. In section 3, we compute chorus-induced scattering rates of Jovian radiation belt electrons and investigate the roles that the initial conditions of electron energy spectrum and pitch angle distribution play in the energetic electron dynamic evolution at Jupiter. We discuss our results and state our conclusions in section 4.

2. Model Description

The present study concentrates on the spatial region of the typically strong radiation environment in the Jovian magnetosphere, i.e., the Jovian L-shells of L_J = 6–14. The adopted models of background magnetic field, plasma density, and wave distribution are specified as follows.

The Jovian magnetic field is reasonably approximated by a dipole model (Khurana, 1997),

$$B = B_{eq}\left(1+3\sin^2\lambda\right)^{1/2}/\cos^6\lambda, \tag{1}$$

where $B_{eq} = B_0/L_J^3$ is the equatorial magnetic field and λ is the magnetic latitude with B_0 = 0.42 mT.

The background plasma density follows (Shprits et al., 2012; Persoon et al., 2006; Ni BB et al., 2018)

$$N(L_J,\lambda) = N_{eq}(L_J)\exp\left(-L_J^2\left(1-\cos^6\lambda\right)/\left(3H^2\right)\right), \tag{2}$$

where

$$N_{eq} = 3.2\times10^8 L_J^{-6.9}\,\mathrm{cm}^{-3} \tag{3}$$

is the equatorial plasma density and $H = 10^{a_1+a_2r+a_3r^2+a_4r^3+a_5r^4}$ with $r = \log_{10}(L_J)$ and a set of parameters a_1 = –0.116, a_2 = 2.14, a_3 = –2.05, a_4 = 0.491, and a_5 = 0.126 (Bagenal and Delamere, 2011).

Regarding the wave frequency spectrum and wave normal angle distribution, we assume that both of them are Gaussian, in accordance with previous studies (e.g., Horne et al., 2008; Ni BB et al., 2008, 2011, 2018; Tao X et al., 2011; Shprits et al., 2012; Thorne et al., 2013). Specifically, the chorus wave power spectral density follows

$$B^2(w) = \begin{cases} A^2\exp\left[-\left(\dfrac{\omega-\omega_m}{\delta\omega}\right)^2\right] & \text{for } \omega_{lc}\le\omega\le\omega_{uc}, \\ 0 & \text{otherwise}, \end{cases} \tag{4}$$

where the term A^2 can be written as

$$A^2 = \frac{2}{\sqrt{\pi}}\frac{|B_w|^2}{\delta\omega}\left(\mathrm{erf}\left(\frac{\omega_m-\omega_{lc}}{\delta\omega}\right)+\mathrm{erf}\left(\frac{\omega_{uc}-\omega_m}{\delta\omega}\right)\right)^{-1}, \tag{5}$$

with ω_{uc} and ω_{lc} as the upper and lower cut-off frequency, ω_m the peak frequency, $\delta\omega$ the spectral band width, and B_w the averaged wave amplitude. The wave normal angle distribution takes the form

$$g(X) = \exp\left(-\left(\frac{X-X_m}{X_\omega}\right)^2\right), \tag{6}$$

where $X = \tan(\theta)$, $X_m = \tan(\theta_m)$, $X_\omega = \tan(\delta\theta)$ with the wave normal angle θ, peak wave normal angle θ_m, and angular width $\delta\theta$. The latitudinal coverage of chorus waves is further assumed to be confined within $|\lambda| < 15°$. The peak wave normal angle follows a latitudinally varying model, i.e., $\theta_m = -0.36+5.04\lambda-0.06\lambda^2$ (Tao X et al., 2011). Table 1 summarizes the inputs for the spectral and wave normal distributions of lower-band and upper-band chorus. These parameters are subsequently utilized to compute the quasi-linear diffusion rates accounting for interactions of Jovian radiation belt electrons with the waves by virtue of the gyroresonance condition that the Doppler-shifted wave frequency experienced by energetic electrons equals a multiple of their gyrofrequency.

Table 1. Lower and upper band chorus wave parameters

		LBC	UBC
Wave spectral intensity profile	ω_m/Ω_{ce}	5×10^{-4}	0.1
	$\delta\omega/\Omega_e$	0.2	0.35
	ω_{lc}/Ω_e	0.03	0.5
	ω_{uc}/Ω_e	0.5	0.8
Wave normal angle distribution	θ_m	$-0.36+5.04\lambda-0.06\lambda^2$	$-0.36+5.04\lambda-0.06\lambda^2$
	$\delta\theta$	30°	15°
	θ_{lc}	0°	0°
	θ_{uc}	50°	30°

3. Analysis Results

The Full Diffusion Code (Ni BB et al., 2008, 2011, 2015) is implemented for various numerical runs to compute the chorus-induced electron scattering rates in the Jovian magnetosphere, for which the contributions from the n = –5 to n = 5 cyclotron harmonic resonances and the Landau resonance (n = 0) are included. With the chorus-induced quasi-linear diffusion coefficients available, we simulate the temporal evolution of the electron phase space density (PSD) in the Jovian radiation belts by numerically solving the 2-D Fokker-Planck diffusion equation,

$$\begin{aligned}\frac{\partial f}{\partial t} =& \frac{1}{p^2}\frac{\partial}{\partial p}\Big|_{\alpha_0,L} p^2\left(\langle D_{pp}(\alpha_0,p)\rangle\frac{\partial f}{\partial p}\Big|_{\alpha_0,L}+\langle D_{p\alpha_0}(\alpha_0,p)\rangle\frac{\partial f}{\partial\alpha_0}\Big|_{p,L}\right)+\frac{1}{T(\alpha_0)\sin(2\alpha_0)}\\ &\frac{\partial}{\partial\alpha_0}\Big|_{p,L} T(\alpha_0)\sin(2\alpha_0)\left(\langle D_{\alpha_0\alpha_0}(\alpha_0,p)\rangle\frac{\partial f}{\partial\alpha_0}\Big|_{p,L}+\langle D_{\alpha_0 p}(\alpha_0,p)\rangle\frac{\partial f}{\partial p}\Big|_{\alpha_0,L}\right)+\frac{f}{\tau},\end{aligned} \tag{7}$$

where f is the electron PSD, t is the time, p is the relativistic momentum (relativistic momentum p can be related to the kinetic energy as $E = \sqrt{p^2c^2+m^2c^4}-mc^2$), α_0 is the equatorial pitch angle, $\langle D_{\alpha\alpha}\rangle$, $\langle D_{pp}\rangle$, and $\langle D_{\alpha p}\rangle$ are the rates of bounce-averaged

pitch angle diffusion, momentum diffusion, and cross diffusion, respectively, and τ is the electron lifetime, which is set as a quarter of the bounce time inside the loss cone and infinite outside the loss cone. $T(\alpha_0)$ is a function related to the particle bounce motion; it is approximated, in a dipolar field, as (Lenchek et al., 1961)

$$T(\alpha_0) = 1.3802 - 0.3198\left(\sin\alpha_0 + \sin^{1/2}\alpha_0\right). \quad (8)$$

To perform numerical simulations of equation (7), the boundary conditions in energy and pitch angle space are set up as follows: the electron PSD is zero inside the equatorial loss cone and $df/d\alpha_0 = 0$ at $\alpha_0 = 90°$; the electron PSDs are equal to the initial values at both the minimum (10 keV for lower band chorus and 1 keV for upper band chorus) and maximum (10 MeV for lower band chorus and 1 MeV for upper band chorus) energy boundaries, which implicitly assumes a balance between the source and loss processes. The 2-D Fokker-Planck equation is solved by a combination of the standard fully implicit method and the standard alternative direction implicit (ADI) method. Readers are referred to the study of Xiao FL et al. (2009) for details of the numerical scheme and method.

3.1 Electron Diffusion Coefficients Due to Lower Band and Upper Band Chorus

Figure 1 shows the latitudinal dependence of B_w over L_J = 6–14 for upper band and lower band chorus, respectively, following the study of Menietti et al. (2016). Clearly, in the Jovian radiation belts the typical wave amplitude is < 20 pT for lower band chorus (LBC) and < 2 pT for upper band chorus (UBC). The LBC wave intensity is strongest at L_J = 12 near the geomagnetic equator and at L_J = 8 at λ > ~5°. In contrast, the UBC wave intensity is most intense at L_J = 8 near the geomagnetic equator and at L_J = 12 and 14 at λ > ~6°. We note that these wave models for lower and upper band chorus are developed to be representative of average wave intensity distributions, which therefore cannot account for the occurrence of stronger chorus waves inside local injection events (Tao X et al., 2011).

Figure 2 displays 2-D plots of quasi-linear bounce-averaged diffusion coefficients of Jovian radiation belt electrons by LBC as a function of equatorial pitch angle and electron kinetic energy for L_J = 6, 8, 10, 12 and 14. It is clearly shown that with the statistically average LBC wave amplitude information provided in Figure 1, LBC can drive efficient pitch angle scattering of a large population of Jovian radiation belt electrons. Specifically, at L_J = 10, 12 and 14, the rates of pitch angle diffusion are above 10^{-5} s^{-1} for electrons of 10 keV to a few MeV. The emissions trigger the most intense pitch angle scattering of ~100 keV–1 MeV electrons at pitch angles ~80°–85° at rates reaching 10^{-4} s^{-1}, mainly due to the Landau resonance. In contrast, the LBC induced scattering rates are < ~10^{-7} s^{-1} at L_J = 6, the region with the weakest wave intensity.

Figure 3 shows 2-D plots of quasi-linear bounce-averaged diffusion coefficients of Jovian radiation belt electrons by UBC, in a manner similar to Figure 2, except for the electron energy range of 1 keV–1 MeV. It is clearly seen that the diffusion rates by UBC are much smaller than those by LBC due to the much weaker in-

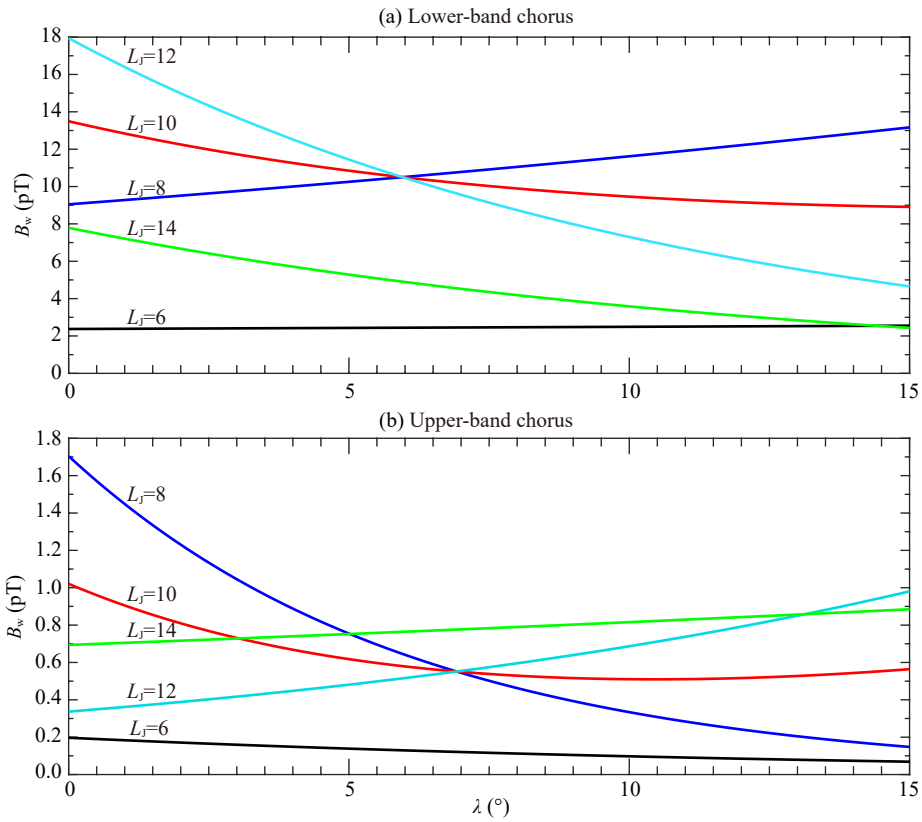

Figure 1. Latitudinal dependence of B_w used in the present study for (a) lower and (b) upper band chorus waves.

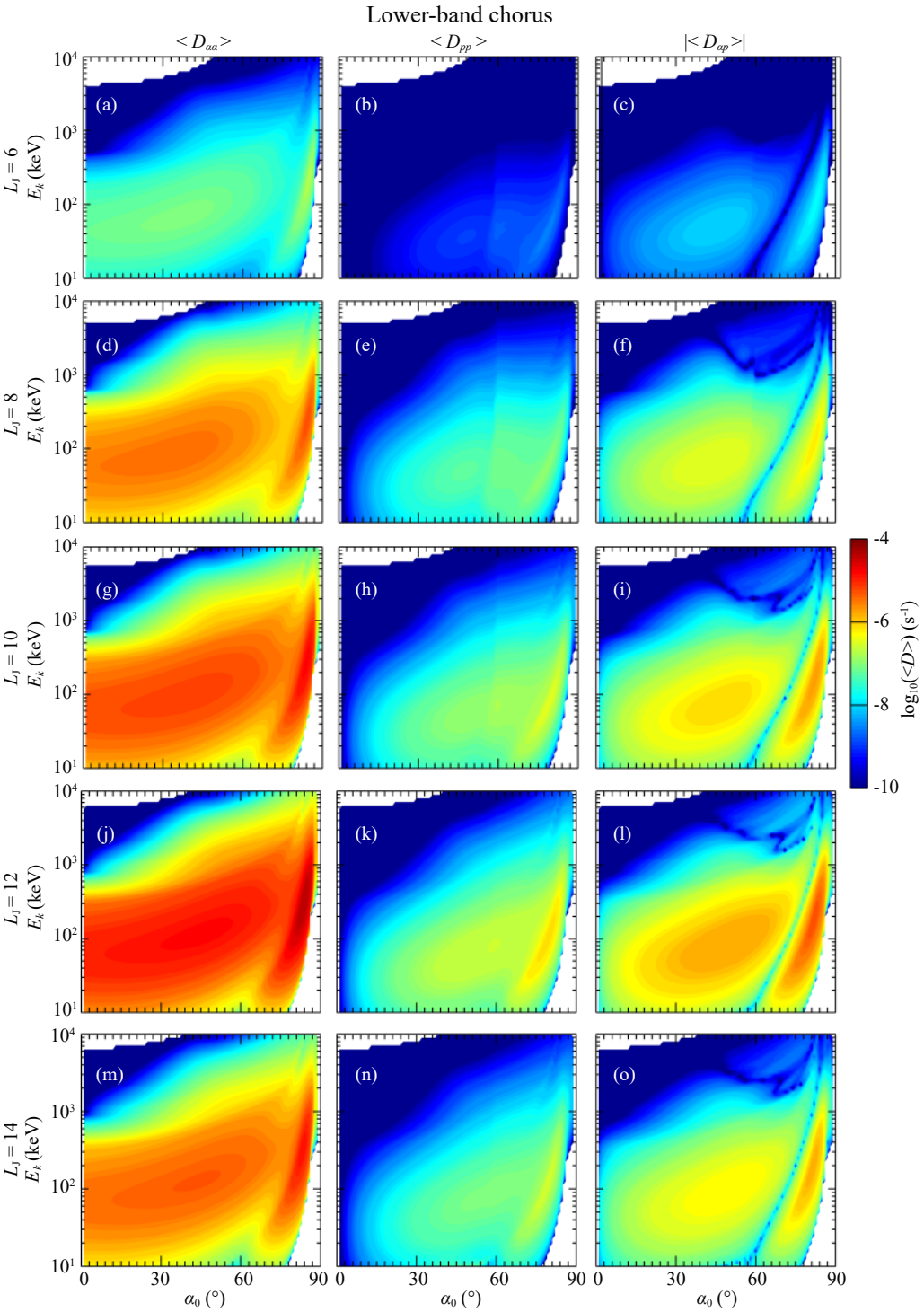

Figure 2. Diffusion coefficients calculated with the FDC code using the lower band chorus wave model in Figure 1a. Each row corresponds to a specific *L*-shell, and the values of three diffusion rates (pitch angle, energy, and mixed diffusion) are given in the left to right columns.

tensity of UBC. In addition, UBC is more likely to cause efficient scattering of electrons of a few keV at lower pitch angles and of ~10–100 keV electrons at intermediate and high pitch angles, with rates well below 10^{-5} s^{-1}.

3.2 Dependence of LBC Induced Electron PSD Variations on Initial Condition

In order to understand how initial conditions influence the PSD, we consider four different distributions of initial phase space energy and pitch angle, and determine how these distributions influence the Jovian radiation belt electron acceleration and loss caused by chorus waves. Figures 4a–d show the profiles of the four initial conditions. Then we select two indicated pitch angle distributions to obtain Figure 4e. Detailed expressions of the considered four initial conditions are as follows:

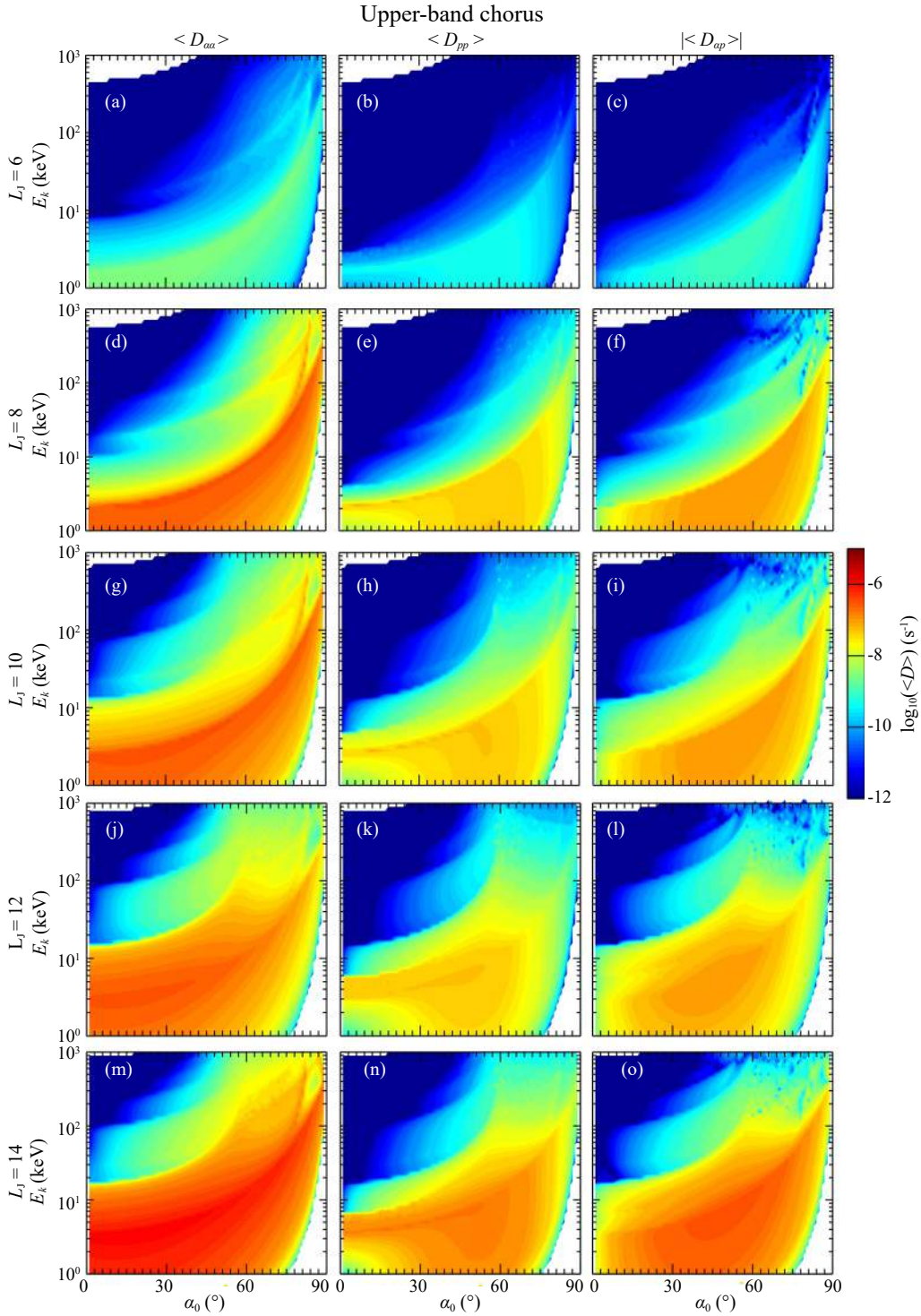

Figure 3. Same as Figure 2 but for upper band chorus waves.

$$\text{Initial Condition 1 (IC\#1)}: j = \exp(-(E-0.2)/0.1)\sin\alpha_0, \quad (9)$$

$$\text{Initial Condition 2 (IC\#2)}: j = \exp(-(E-0.2)/0.1), \quad (10)$$

$$\text{Initial Condition 3 (IC\#3)}: j = 10^{10}\left(L^{-4}/E\right), \quad (11)$$

$$\text{Initial Condition 4 (IC\#4)}: j = 10^{10}\left(L^{-4}/E\right)\sin\alpha_0. \quad (12)$$

IC #1 is adopted from the study of de Soria-Santacruz et al. (2017), and IC #3 from the study of Tomás et al. (2004); the kinetic energy E is given in unit of keV and the electron flux is given in unit of $cm^{-2}sr^{-1}s^{-1}keV^{-1}$. Based on Initial Conditions #1 and #3, we further adopt Initial Conditions #2 and #4 for quantitative analyses. It is clear from Figure 4e that Initial Conditions #1 and #2 have larger gradients at higher energies and that all the initial electron PSDs decrease with increasing energy.

Figure 5 shows the temporal evolution of electron PSD as a func-

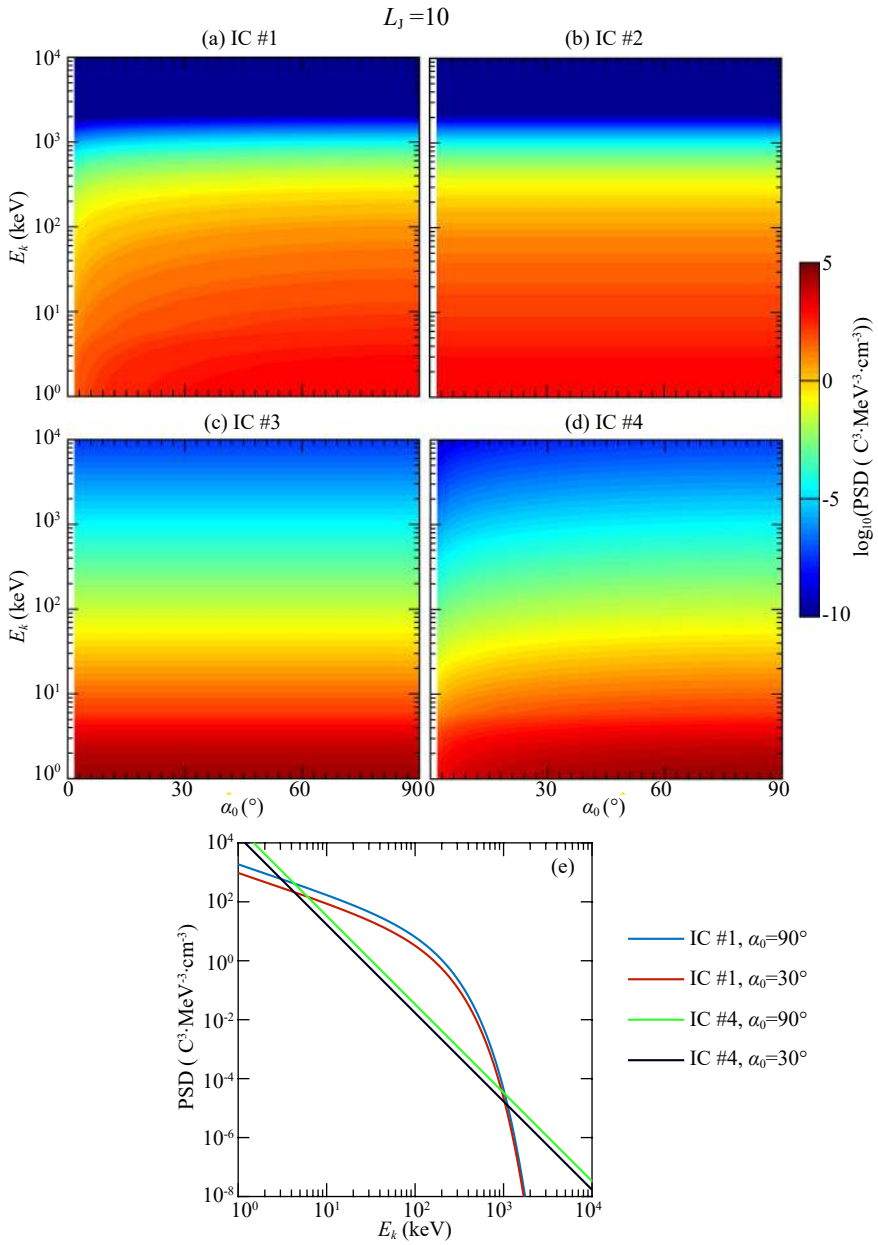

Figure 4. Four initial conditions used in this study (a–d). Two examples of the pitch angle distribution (α_0=30° and α_0=90°) of electron PSD are shown in (e).

tion of equatorial pitch angle under the impact of lower-band chorus waves at L_J=10. Each row corresponds to one of the four considered initial conditions described in section 3.2, and each column corresponds to a considered electron energy. Specifically, we choose 6 energies, i.e., 12 keV, 30 keV, 100 keV, 500 keV, 1 MeV and 5 MeV to study the energy dependence of chorus induced diffusion. The evolution time is 10 days. For 12 keV electrons, there occurs some electron acceleration for Initial Conditions #3 and #4 at pitch angles ~45°–65°. However, for Initial Conditions #1 and #2, the acceleration is almost negligible. There is particle loss at pitch angles <~45° and >~65° for all considered initial conditions. For 30 keV and 100 keV electrons, chorus wave diffusion leads to particle losses for all initial conditions. Electrons of 500 keV get accelerated at all pitch angles for Initial Condition #1; for Initial Condition #2 they get lost at pitch angles <~10° and accelerated at pitch angles >~10°; for Initial Condition #3 they get lost at almost all pitch angles for Initial Condition #4 they get accelerated at pitch angles <~30° and lost at pitch angles >~30°. Electrons of 1 MeV get accelerated at all pitch angles for Initial Condition #1; get accelerated at pitch angles >~10° and remain almost unchanged at pitch angles <~10° for Initial Condition #2; keep unchanged at all pitch angles for Initial Condition #3; and get accelerated at pitch angles <~40° and lost at pitch angles >~40° for Initial Condition #4. Electrons of 5 MeV remain almost unchanged at all pitch angles for Initial Conditions #3 and #4, and get accelerated at pitch angles >~40° for Initial Condition #1 and #2. Checking the effect of varying initial pitch angle distributions of electron PSD, we find that inclusion of pitch angle variation in

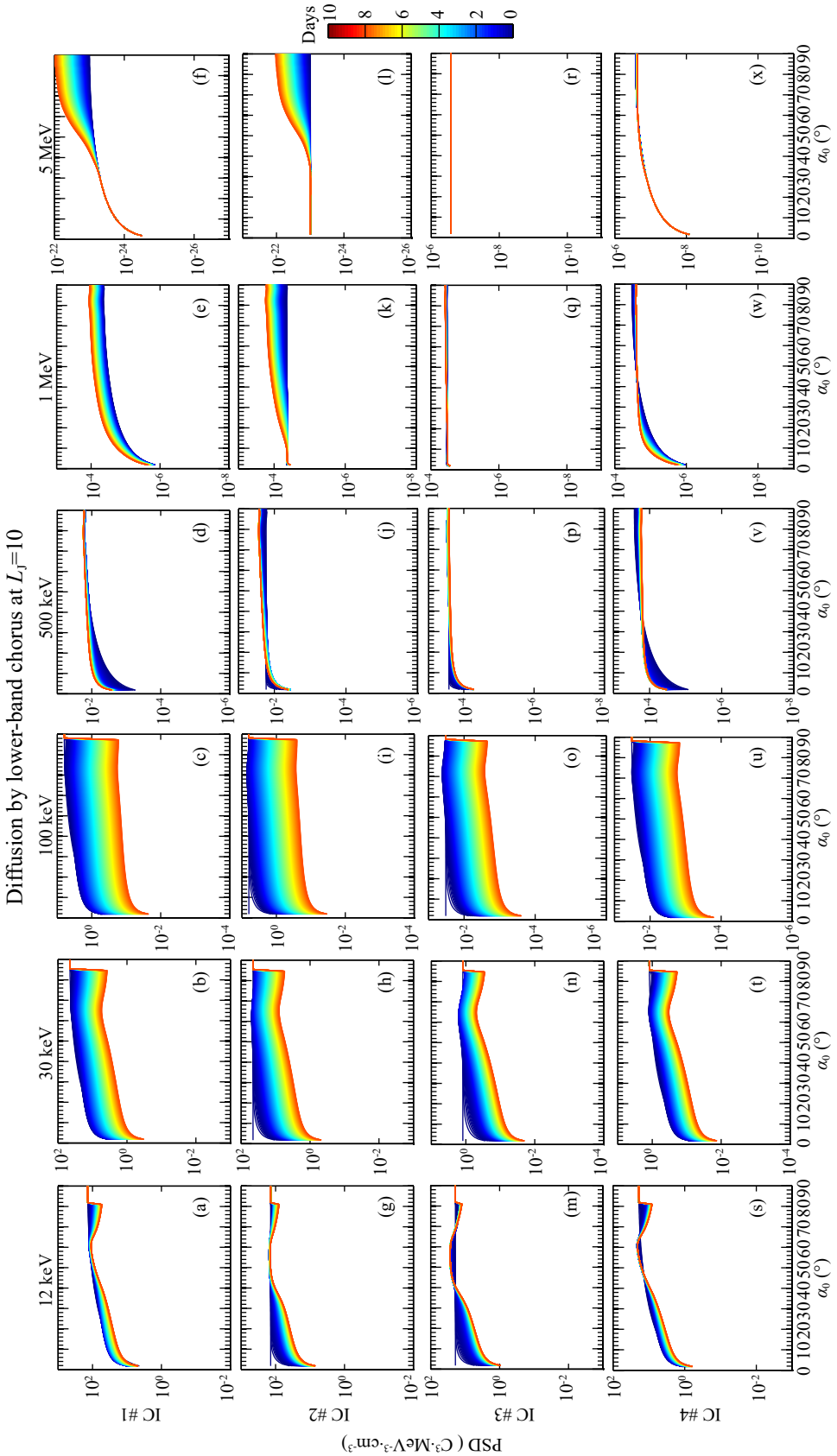

Figure 5. Evolution of electron PSD for the lower band chorus at L_J=10. Each row corresponds to one of the adopted initial conditions, and each column corresponds to an electron energy.

Initial Conditions #1 and #4 can result in increased electron losses at lower pitch angles; and pitch angle evolution profiles of 500 keV, 1 MeV and 5 MeV electrons can be substantially modified. In contrast, checking the effect of varying initial electron energy spectra, we find that such variations tend to modify the evolution primarily of 1 MeV and 5 MeV electrons.

In order to evaluate the differences in electron PSD profile that different initial pitch angle distributions can produce, we compute the relative difference (RD) between model results, the expression of which follows

$$\mathrm{RD} = \mathrm{PSD}_{\mathrm{IC\#A}}/\mathrm{PSD}_{\mathrm{IC\#B}}. \tag{13}$$

Figure 6 shows the RD results for Jovian radiation belt electron PSD evolution under the impact of lower-band chorus. Each row corresponds to a considered L_J and each column corresponds to a different value of A and B. The first two columns correspond to the evolution time of 1 day and the other two columns correspond to the evolution time of 10 days. It is shown that the RD is largest for > ~600 keV electrons at pitch angles < ~15°; RD is small at other electron energies and pitch angles. As L_J increases, the RD profile does not change in obvious ways. In addition, as the evolution time increases, the RD becomes weaker for ~600 keV–2 MeV electrons at pitch angles < ~15°.

Regarding the RD introduced by varying the initial energy spectra, since the two adopted energy spectra differ substantially from each other, we first normalize the electron PSD evolution results by the initial profile and then compute the relative differences; that is,

$$\mathrm{NPSD} = \mathrm{PSD}/\mathrm{PSD}_{\mathrm{initial}}, \tag{14}$$

and

$$\mathrm{NRD} = \mathrm{NPSD}_{\mathrm{IC\#A}}/\mathrm{NPSD}_{\mathrm{IC\#B}}, \tag{15}$$

where NPSD is the normalized electron PSD and NRD is the corresponding relative difference. Figure 7A displays the results for use of Initial Conditions #1 and #4 with evolution time of 1 day. The difference is almost negligible except in the regions of ~10–100 keV electrons at pitch angles <~35° and ~50°–80°, and ~300 keV–10 MeV electrons at pitch angles ~45°–90°. As L_J increases, the relative difference becomes larger while the trend profiles are similar. Figure 7B shows the results with evolution time of 10 days. Clearly, the region with obvious differences expands with increasing evolution time. Specifically, in the regions of ~10–100 keV electrons at pitch angles < ~80°, and ~300 keV–10 MeV electrons at pitch angles ~30°–90°, the difference is evident. Similarly, the difference also increases with L_J.

3.3 Dependence of UBC Induced Electron PSD Variations on Initial Condition

Similar to Figure 5, Figure 8 shows the electron PSD evolution under the impact of upper-band chorus waves at L_J=10. We con-

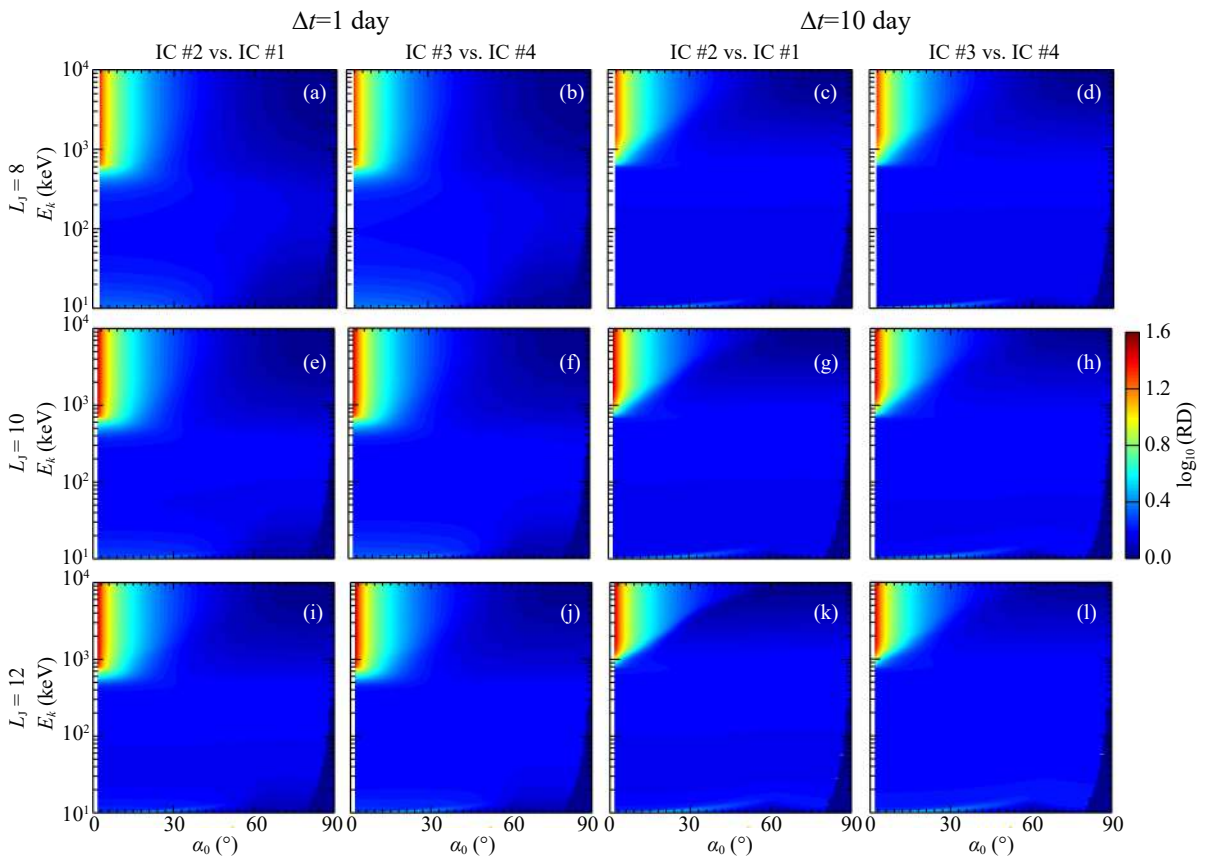

Figure 6. The relative differences in the electron PSD temporal evolution caused by the lower-band chorus scattering under different initial pitch angle distributions for the evolution time periods of 1 day and 10 days. Each row corresponds to a specific *L*-shell.

sider the electron energies of 1.5 keV, 5 keV, 10 keV, 50 keV, 100 keV, and 500 keV. Overall, the electron PSD variations caused by upper band chorus in the Jovian radiation belt are smaller than those caused by lower band chorus. Electrons of 1.5keV get accelerated at pitch angles <~15° and >~60° and lost at pitch angles ~15°–60° for Initial Condition #1; for Initial Conditions #2, #3, and #4 they get lost at pitch angles < ~45° and accelerated at pitch angles > ~45°. Electrons of 5 keV get accelerated at pitch angles < ~30° and > ~70° and lost at pitch angles ~30°–70° for Initial Condition #1; for Initial Condition #2 they get lost at pitch angles < ~50° and accelerated at pitch angles > ~50°; for Initial Condition #3 they get lost at pitch angles < ~30° and accelerated at pitch angles > ~30°; for Initial Condition #4 they get accelerated at almost all pitch angles. Electrons of 10 keV undergo slight losses at almost all pitch angles for Initial Condition #1; they get lost at pitch angles < ~10° and accelerated at pitch angles > ~60° for Initial Condition #2; they get lost at pitch angles < ~10° and accelerated at pitch angles > ~50° for Initial Condition #3; and for Initial Condition #4 they get accelerated at almost all pitch angles. Electrons of 50 keV remain almost unchanged at all pitch angles for Initial Conditions #1 and #2, and get slightly accelerated at pitch angles > ~70° for Initial Conditions #3 and #4. Electrons of 100 keV and 500 keV are almost unchanged at all pitch angles for all considered initial conditions.

Figure 9 shows the RD results in a manner similar to Figure 6, except for upper-band chorus. These results exhibit relative differences patterns similar to those for lower-band chorus. The differences are largest in the region of > ~2 keV electrons at pitch angles < ~15°, and deepen with increasing evolution time but become smaller with increasing L_J. In contrast, Figure 10 shows the RD results caused by varying initial energy spectra under the impact of upper band chorus. It is shown that the differences are large at energies < ~5 keV and ~20–500 keV, and again increase with evolution time but decrease with L_J.

4. Discussions and Conclusions

We have analyzed the effect of realistic chorus waves in the Jovian magnetosphere on the dynamics of radiation belt energetic electrons. In contrast to previous studies of wave-particle interactions at Jupiter that were based on preliminary chorus measurements (Horne et al., 2008) and lacked the information of spectral and spatial parameters (Shprits et al., 2012; Woodfield et al., 2013, 2014), in the present study we have incorporated the set of this

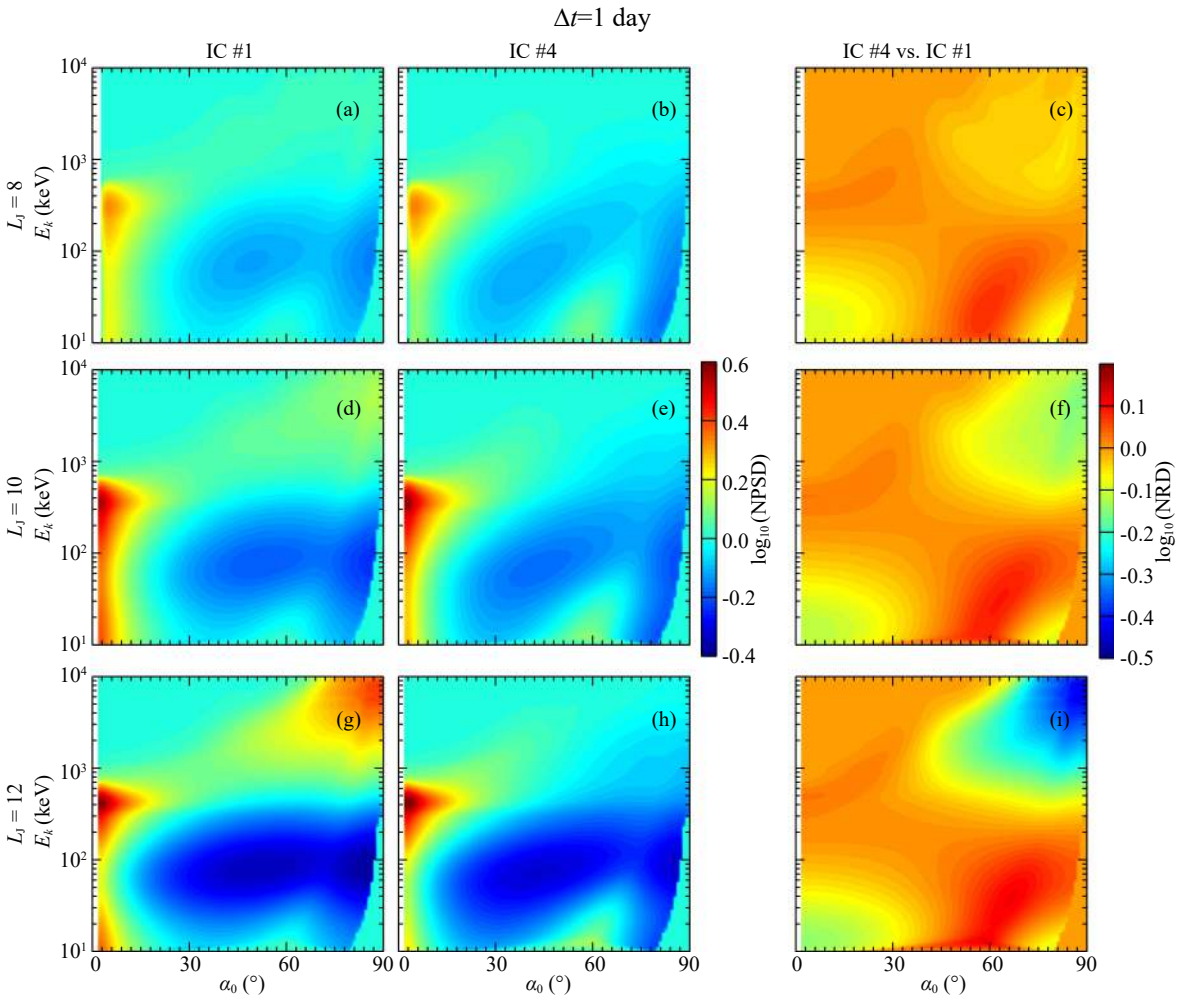

Figure 7A. Normalized electron PSD evolution and corresponding relative differences under the impact of lower band chorus with the 1-day evolution time for the two pitch angle distributions of initial conditions and indicated L_J-values.

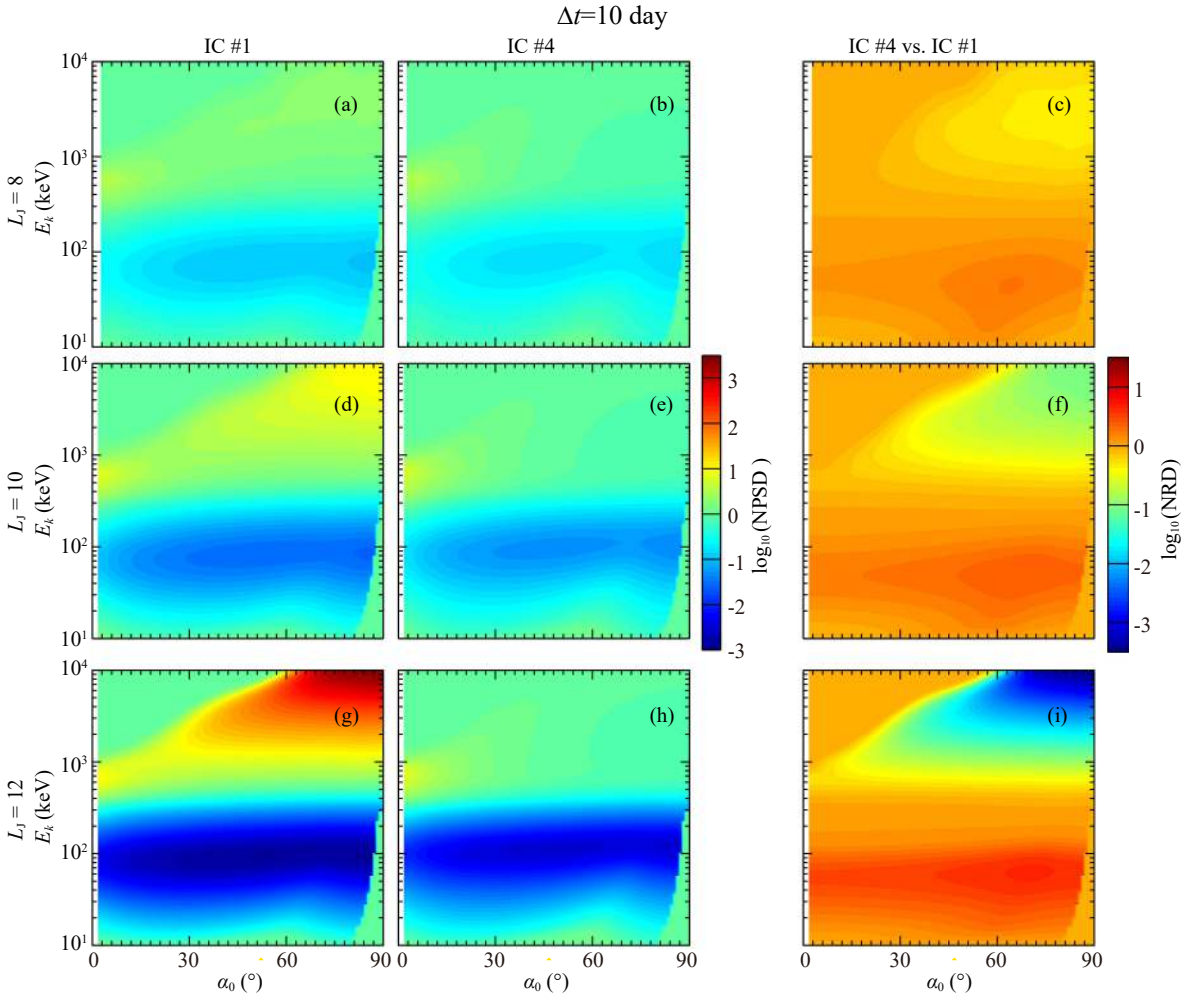

Figure 7B. Same as Figure 7A but for the evolution time of 10 days.

important information based on the extensive survey of chorus waves by Menietti et al. (2016). In order to understand how initial conditions influence the evolution of electron phase space density, we have adopted a sample of four reasonable initial conditions to investigate in detail how initial electron energy spectra and pitch angle distributions can influence electron acceleration and loss processes in the Jovian radiation belt.

Our main conclusions are summarized as follows:

(1) Due to the Landau resonance between the chorus waves and electrons, the emissions can cause more intense pitch angle scattering of ~10 keV–1 MeV electrons at pitch angles ~70°–80° for lower-band chorus.

(2) For lower-band chorus, the initial conditions with different energy spectra can cause the electron acceleration of 500 keV and 1 MeV electrons at lower pitch angles, and different initial pitch angle distributions can cause 1 MeV and 5 MeV electron acceleration at high pitch angles.

(3) For upper-band chorus, different initial energy spectra can cause the acceleration of 5 keV and 10 keV electrons at lower pitch angles, and different initial pitch angle distributions can cause ~1.5–50 keV electron acceleration at high pitch angles.

Our detailed analysis demonstrates the importance of the shape of electron phase space density to the dynamic variations of Jovian radiation belt electrons, which exhibit strong and complex dependence on electron energy, pitch angle, and spatial location. It is found that quasi-linear electron scattering rates by chorus can be strongly affected by the ambient magnetic field intensity, the wave latitudinal coverage, and the peak frequency and bandwidth of the wave spectral distribution in the Jovian magnetosphere, while scattering rates rely only slightly on the background plasma density profile and the peak wave normal angle, especially when the wave emissions are confined at lower latitudes. In addition, the initial electron energy spectrum and pitch angle distribution can obviously influence the electron acceleration and loss processes in the Jovian radiation belt. When wave and particle measurements from the Juno spacecraft are released publicly, further analysis will be undertaken to improve understanding of the interactions between chorus waves and Jovian radiation belt electron acceleration.

Acknowledgments

This work was supported by NSFC grants (41674163) and (41474141), and by the Hubei Province Natural Science Excellent

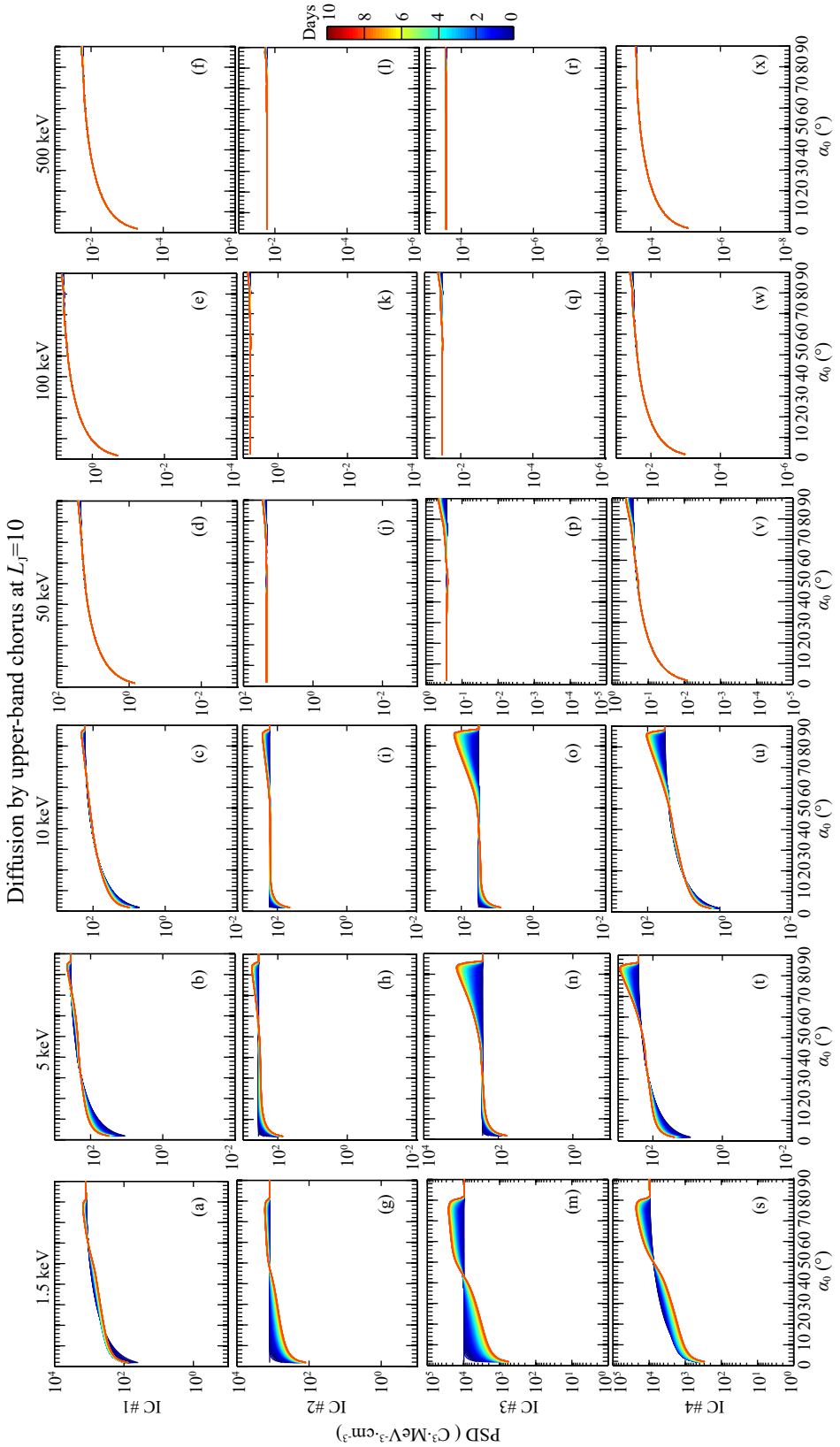

Figure 8. Same as Figure 5 but for upper band chorus waves.

Youth Foundation (2016CFA044). X. D. Gu and B. B. Ni also acknowledge the open-fund grant by the Lunar and Planetary Science Laboratory, Macau University of Science and Technology Partner Laboratory of Key Laboratory of Lunar and Deep Space Exploration, Chinese Academy of Sciences.

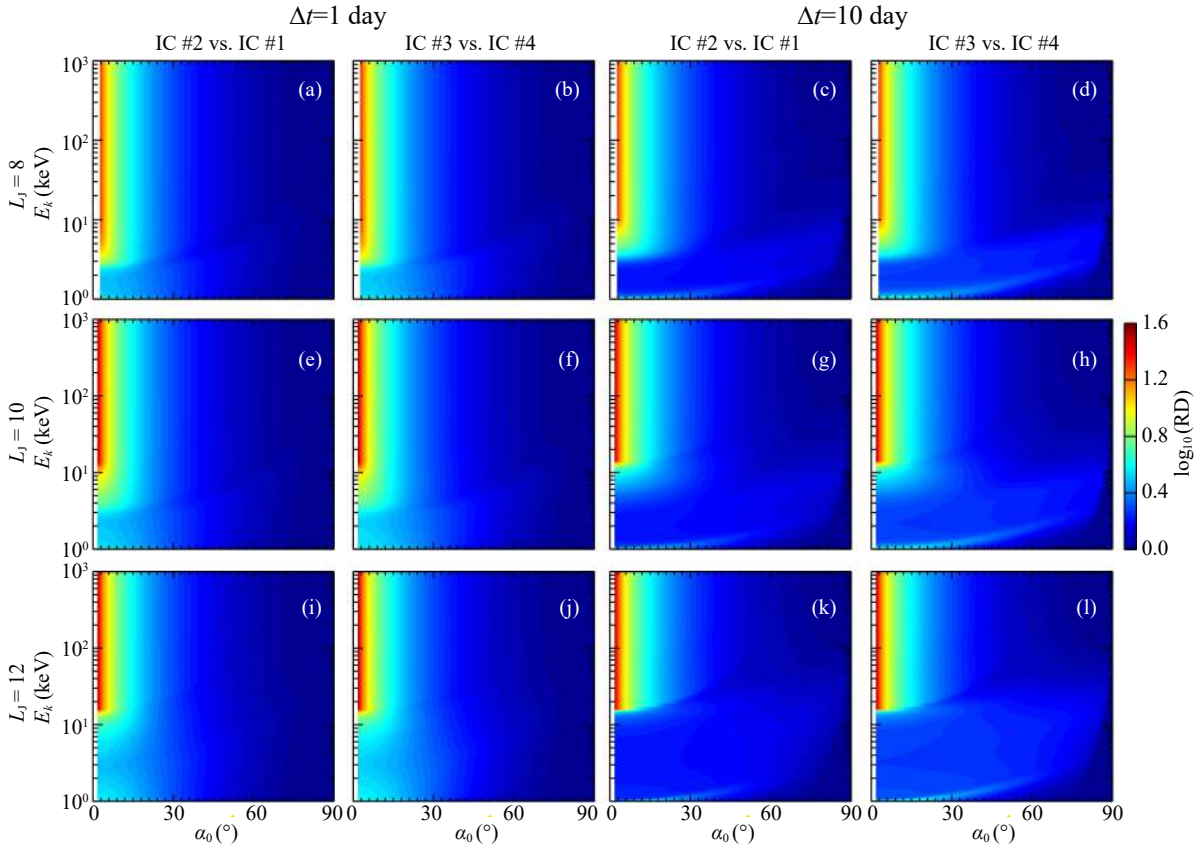

Figure 9. Same as Figure 6 but for upper band chorus waves.

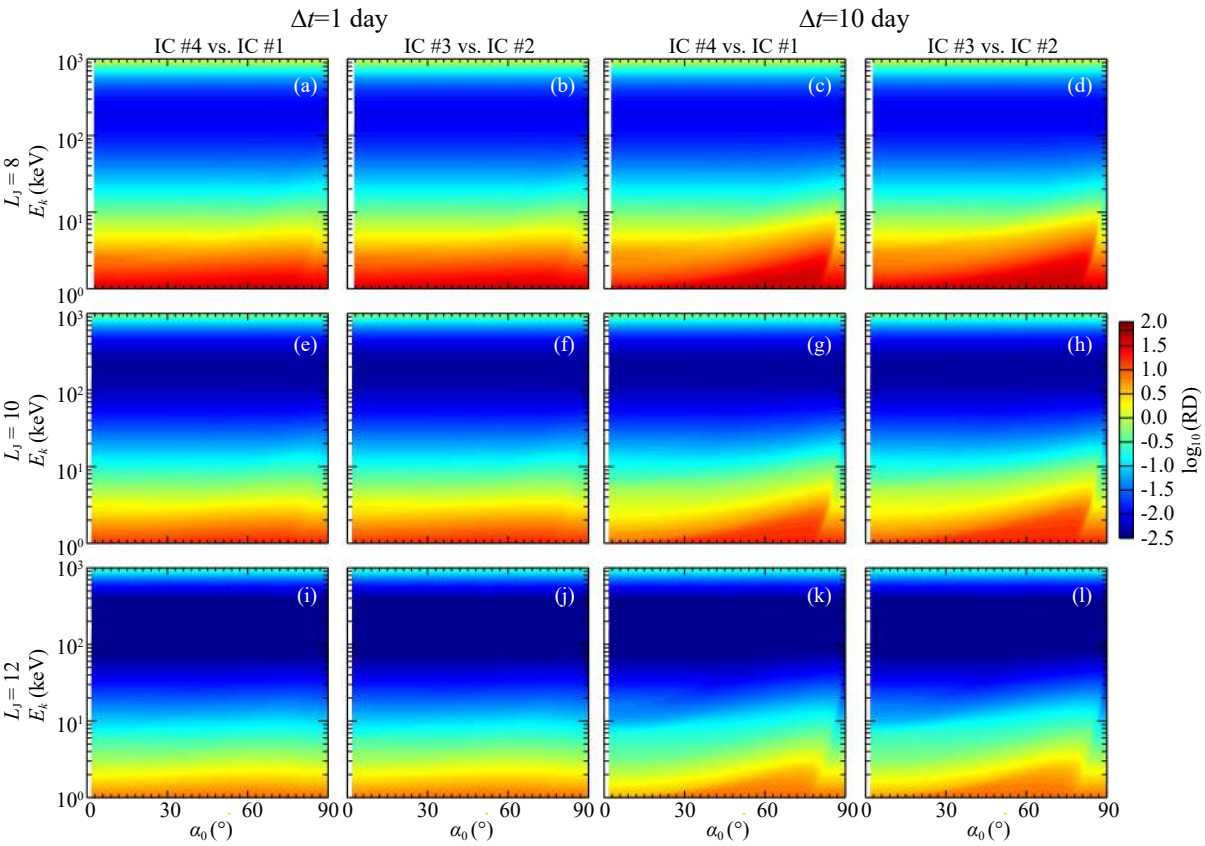

Figure 10. Same as Figure 9 but for varying initial energy spectra.

References

Bagenal, F., and Delamere, P. A. (2011). Flow of mass and energy in the magnetospheres of Jupiter and Saturn. *J. Geophys. Res.*, *116*(A5), A05209. https://doi.org/10.1029/2010JA016294

Bolton, S. J., Janssen, M., Thorne, R., Levin, S., Klein, M., Gulkis, S., Bastian, T., Sault, R., Elachi, C., … West, R. (2002). Ultra-relativistic electrons in Jupiter's radiation belts. *Nature*, *415*(6875), 987–991. https://doi.org/10.1038/415987a

Carr, T. D., and Gulkis, S. (1969). The magnetosphere of Jupiter. *Annu. Rev. Astron. Astrophys.*, *7*, 577–618. https://doi.org/10.1146/annurev.aa.07.090169.003045

de Soria-Santacruz, M., Shprits, Y. Y., Drozdov, A., Menietti, J. D., Garrett, H. B., Zhu, H., Kellerman, A. C., and Horne, R. B. (2017). Interactions between energetic electrons and realistic whistler mode waves in the Jovian magnetosphere. *J. Geophys. Res.*, *122*(5), 5355–5364. https://doi.org/10.1002/2017JA023975

Horne, R. B., Thorne, R. M., Glauert, S. A., Menietti, J. D., Shprits, Y. Y., and Gurnett, D. A. (2008). Gyro-resonant electron acceleration at Jupiter. *Nat. Phys.*, *4*(4), 301–304. https://doi.org/10.1038/nphys897

Khurana, K. K. (1997). Euler potential models of Jupiter's magnetospheric field. *J. Geophys. Res.*, *102*(A6), 11295–11306. https://doi.org/10.1029/97JA00563

Lenchek, A. M., Singer, S. F., and Wentworth, R. C. (1961). Geomagnetically trapped electrons from cosmic ray albedo neutrons. *J. Geophys. Res.*, *66*(12), 4027–4046. https://doi.org/10.1029/JZ066i012p04027

Menietti, J. D., Groene, J. B., Averkamp, T. F., Horne, R. B., Woodfield, E. E., Shprits, Y. Y., de Soria-Santacruz Pich, M., and Gurnett, D. A. (2016). Survey of whistler mode chorus intensity at Jupiter. *J. Geophys. Res.*, *121*(10), 9758–9770. https://doi.org/10.1002/2016JA022969

Ni, B. B., Thorne, R. M., Shprits, Y. Y., and Bortnik, J. (2008). Resonant scattering of plasma sheet electrons by whistler-mode chorus: Contribution to diffuse auroral precipitation. *Geophys. Res. Lett.*, *35*(11), L11106. https://doi.org/10.1029/2008GL034032

Ni, B. B., Thorne, R. M., Meredith, N. P., Horne, R. B., and Shprits, Y. Y. (2011). Resonant scattering of plasma sheet electrons leading to diffuse auroral precipitation: 2 Evaluation for whistler mode chorus waves. *J. Geophys. Res.*, *116*(A4), A04219. https://doi.org/10.1029/2010JA016233

Ni, B. B., Cao, X., Zou, Z. Y., Zhou, C., Gu, X. D., Bortnik, J., Zhang, J. C., Fu, S., Zhao, Z. Y., … and Xie, L. (2015). Resonant scattering of outer zone relativistic electrons by multiband EMIC waves and resultant electron loss time scales. *J. Geophys. Res.*, *120*(9), 7357–7373. https://doi.org/10.1002/2015JA021466

Ni, B. B., Huang, J., Ge, Y. S., Cui, J., Wei, Y., Gu, X. D., Fu, S., Xiang, Z., and Zhao, Z. Y. (2018). Radiation belt electron scattering by whistler-mode chorus in the Jovian magnetosphere: Importance of ambient and wave parameters. *Earth Planet. Phys.*, *2*(1), 1–14. https://doi.org/10.26464/epp2018001

Persoon, A. M., Gurnett, D. A., Kurth, W. S., and Groene, J. B. (2006). A simple scale height model of the electron density in Saturn's plasma disk. *Geophys. Res. Lett.*, *33*(18), L18106. https://doi.org/10.1029/2006GL027090

Shprits, Y. Y., Menietti, J. D., Gu, X., Kim, K. C., and Horne, R. B. (2012). Gyroresonant interactions between the radiation belt electrons and whistler mode chorus waves in the radiation environments of Earth, Jupiter, and Saturn: A comparative study. *J. Geophys. Res.*, *117*(A11), A11216. https://doi.org/10.1029/2012JA018031

Tao, X., Thorne, R. M., Horne, R. B., Ni, B., Menietti, J. D., Shprits, Y. Y., and Gurnett, D. A. (2011). Importance of plasma injection events for energization of relativistic electrons in the Jovian magnetosphere. *J. Geophys. Res.*, *116*(A01), A01206. https://doi.org/10.1029/2010JA01610

Thorne, R. M., Li, W., Ni, B., Ma, Q., Bortnik, J., Baker, D. N., Spence, H. E., Reeves, G. D., Henderson, M. G., … Angelopoulos, V. (2013). Evolution and slow decay of an unusual narrow ring of relativistic electrons near L ~ 3.2 following the September 2012 magnetic storm. *Geophys. Res. Lett.*, *40*(14), 3507–3511. https://doi.org/10.1002/grl.50627

Tomás, A. T., Woch, J., Krupp, N., Lagg, A., Glassmeier, K. H., and Kurth, W. S. (2004). Energetic electrons in the inner part of the Jovian magnetosphere and their relation to auroral emissions. *J. Geophys. Res.*, *109*(A6), A06203. https://doi.org/10.1029/2004JA010405

Woodfield, E. E., Horne, R. B., Glauert, S. A., Menietti, J. D., and Shprits, Y. Y. (2013). Electron acceleration at Jupiter: Input from cyclotron-resonant interaction with whistler-mode chorus waves. *Ann. Geophys.*, *31*(10), 1619–1630. https://doi.org/10.5194/angeo-31-1619-2013

Woodfield, E. E., Horne, R. B., Glauert, S. A., Menietti, J. D., and Shprits, Y. Y. (2014). The origin of Jupiter's outer radiation belt. *J. Geophys. Res.*, *119*(5), 3490–3502. https://doi.org/10.1002/2014JA019891

Xiao, F. L., Su, Z. P., Zheng, H. N., and Wang, S. (2009). Modeling of outer radiation belt electrons by multidimensional diffusion process. *J. Geophys. Res.*, *114*(A3), A03201. https://doi.org/10.1029/2008JA013580